Geophysics and Thermodynamics at South Pole Lake Indicate Stability and a Regionally Thawed Bed

Benjamin H. Hills[1,2] , Knut Christianson[1] , Andrew O. Hoffman[1,2] , T. J. Fudge[1] , Nicholas Holschuh[3] , Emma C. Kahle[1] , Howard Conway[1] , John E. Christian[1,4,5] , Annika N. Horlings[1], Gemma K. O'Connor[1] , and Eric J. Steig[1]

[1]Department of Earth and Space Sciences, University of Washington, Seattle, WA, USA, [2]Applied Physics Laboratory, Polar Science Center, University of Washington, Seattle, WA, USA, [3]Department of Geology, Amherst College, Amherst, MA, USA, [4]Department of Earth and Atmospheric Sciences, Georgia Institute of Technology, Atlanta, GA, USA, [5]Jackson School of Geosciences, University of Texas at Austin, Austin, TX, USA

Abstract Subglacial lakes require a thawed bed either now or in the past; thus, their presence and stability have implications for current and past basal conditions, ice dynamics, and climate. Here, we present the most extensive geophysical exploration to date of a subglacial lake near the geographic South Pole, including radar-imaged stratigraphy, surface velocities, and englacial vertical velocities. We use a 1.5-dimensional temperature model, optimized with our geophysical data set and nearby temperature measurements, to estimate past basal-melt rates. The ice geometry, reflected bed-echo power, surface and vertical velocities, and temperature model indicate that the ice-bed interface is regionally thawed, contradicting prior studies. Together with an earlier active-source seismic study, which showed a 32-m deep lake underlain by 150 m of sediment, our results suggest that the lake has been thermodynamically stable through at least the last 120,000 years and possibly much longer, making it a promising prospective site for sediment coring.

Plain Language Summary There are hundreds of subglacial lakes under the Antarctic Ice Sheet. The presence of those lakes requires sufficient heat, sourced either from the Earth's interior or from ice motion. One subglacial lake near the South Pole was previously considered a conundrum since nearby temperature measurements are cold, possibly indicating that the ice should be frozen to the surface below it. Here, we use radar and velocity measurements to better understand the ice-sheet geometry, ice motion, and the nature of the underlying bed. We find that the lake is currently filled to within 2 m of its maximum capacity and that the entire surveyed area likely has a thawed bed. We then use nearby measurements of ice temperature and historical climate data from the South Pole Ice Core to calculate the past temperatures of the ice. These calculations indicate a thawed bed. We suggest that the lake has been thermally stable for at least the last 120,000 years and possibly much longer. A prior study showed that the lake is underlain by 150 m of sediment, making it a candidate for sediment coring.

1. Introduction

The existence of a subglacial lake requires that the base of the ice sheet is, or has been, thawed. Lakes can thus provide windows into past regional ice dynamics and climate. South Pole Lake (SPL) is a subglacial lake in East Antarctica that was first detected in the Pensacola Pole Transect (Carter et al., 2007), though it had been imaged in earlier radar surveys (Siegert et al., 2005). This lake is only 10 km from the South Pole Ice Core, which provides well-constrained climate data over the last 50 ka (Kahle et al., 2021; Steig et al., 2021). There are 150 m of sediment beneath the lake (Peters et al., 2008). In this region of the East Antarctic interior, which has likely been glaciated for much of the last 35 million years (Deconto & Pollard, 2003; Siegert, 2008), such lake sediments could extend the recorded climate and geologic history far beyond the ∼800-ka record preserved in ice cores, potentially to before Antarctic glaciation. Thus, this site is a promising target for sediment-core paleoclimate studies (Christoffersen et al., 2008; Kuhn et al., 2017; Smith et al., 2018).

The thermodynamic stability of SPL and the regional ice flow history play key roles in determining the sedimentation history beneath the lake. Nearby temperature measurements have been used to infer a regionally frozen bed (Price et al., 2002), supporting a hypothesis that SPL is a remnant of the past ice sheet and is freezing today (Beem et al., 2017). This hypothesis was based on radar evidence for a possible past upstream extension of Support Force

Resources: Benjamin H. Hills, Emma C. Kahle, Howard Conway
Software: Benjamin H. Hills
Supervision: Knut Christianson, T. J. Fudge
Validation: Benjamin H. Hills, Howard Conway
Visualization: Benjamin H. Hills, Nicholas Holschuh, Emma C. Kahle, Howard Conway
Writing – original draft: Benjamin H. Hills
Writing – review & editing: Benjamin H. Hills, Knut Christianson, Andrew O. Hoffman, T. J. Fudge, Nicholas Holschuh, Emma C. Kahle, Howard Conway, John E. Christian, Annika N. Horlings, Gemma K. O'Connor, Eric J. Steig

Ice Stream toward the South Pole region that persisted until as recently as 10,000 years ago. The radar evidence for a paleo ice stream comes from two separate observations: disruptions in the englacial stratigraphy (Bingham et al., 2007), and higher submergence rates (Beem et al., 2017) within the inferred ice-stream extension.

Here, we present a new ground-based geophysical survey at SPL. Our survey constrains the current ice-sheet geometry, bed properties, and ice dynamics at higher resolution than previous work. With a more thorough description of the lake setting and newly acquired paleoclimate constraints from the recently drilled and nearby South Pole Ice Core, we offer an updated hypothesis that SPL is in fact thermodynamically stable under current conditions.

2. Geophysical Methods and Results

2.1. Ice Sheet and Lake Geometry

We collected 150 line-km of ground-based 3-MHz impulse radar data (Figure 1). Hills et al. (2020) detail the data processing. We estimate the ice thickness by digitizing the bed reflection in each profile using a semiauto-mated routine built in the radar processing and interpretation package ImpDAR (Lilien et al., 2020). Absolute range uncertainty is roughly ¼ wavelength (14 m), while the relative uncertainty from crossover analysis is ∼1 m (Hills et al., 2020). Generally, englacial layers are bed-conformal and nearly flat, but two features stand out. First, a shallow angular unconformity cross cuts layers between the surface and 300-m depth (Figures 2a and S5 in Supporting Information S1). This unconformity dips in the direction of ice flow, to the grid northwest, with a slope 7.5 m/km (as expected, this is approximately equal to the accumulation rate divided by the downstream velocity). Second, we observe a synclinal depression with its fold axis oriented in the direction of ice flow along the grid southwest of the lake (Figures 2a and S7 in Supporting Information S1). This feature is present in most profiles and has a consistent morphology; it is ∼2-km wide and 200-m tall from ridge to trough. The syncline starts upstream of the lake, leading us to believe that it is not a lake feature, unlike past observations of lake-derived stratigraphy (e.g., Tikku et al., 2004).

Given the limited satellite elevation data near the South Pole, we also surveyed the surface elevation using Global Navigation Satellite System (GNSS) kinematic profiling. We collected approximately 1,000 line-km of dual-frequency GNSS data, using Septentrio Altus APS3G receivers sampling at 1 Hz along transects spaced 1 km apart. The antenna was mounted on an aluminum pole attached to a snowmobile that extended ∼2 m above the snow surface. Position uncertainties are 5 cm or less in all dimensions.

We use spline interpolation between the radar and GNSS profiles to generate bed and surface elevation grids (Supporting Information S1). We use our interpolated bed and surface elevation fields to calculate the glacio-static hydropotential (Shreve, 1972). The hydropotential basin at the center of the surveyed area is the site of the subglacial lake. We define the exact lake boundary as the most conservative; i.e., the lowest basin which encircles the liquid water imaged in the seismic data (Peters et al., 2008).

The center of SPL is 12 km to the grid south and 8 km to the grid west of the geographic South Pole along 150°W longitude. The bed elevation is depressed by 150 m at the site of the lake with an upsloping bed to the grid west, north, and east. The bed depression extends to the grid southwest. The surface elevation is depressed at the lake site by 10 m. Opposite to the bed, the surface depression continues as a trough to the grid north, but it is bounded by surface highs to the grid west, south, and east. The hydropotential shows a basin at the lake site with an upstream inlet to the grid east and outflow to the grid south, but a 100-kPa hydropotential barrier perpendicular to ice flow. We refer to this hydropotential barrier as "the ridge." Our data indicate that the lake overflow level at the southern outlet is 20 kPa above the conservative lakestand that we outlined (or ∼2 m water equivalent). Small, currently active outflows may not be detected by this radar, since it has a large footprint (the first Fresnel zone is ∼420-m wide at this ice thickness).

2.2. Bed-Echo Power

Beyond the radar processing described by Hills et al. (2020), we apply additional corrections to the measured bed-echo power for attenuative losses using an Arrhenius model (MacGregor et al., 2007), which was tuned to match the empirically calculated attenuation rates (Hills et al., 2020). Bed-echo power over the surveyed area is normally distributed, showing no consistent spatial patterns (Figure 2). The difference between mean bed-echo
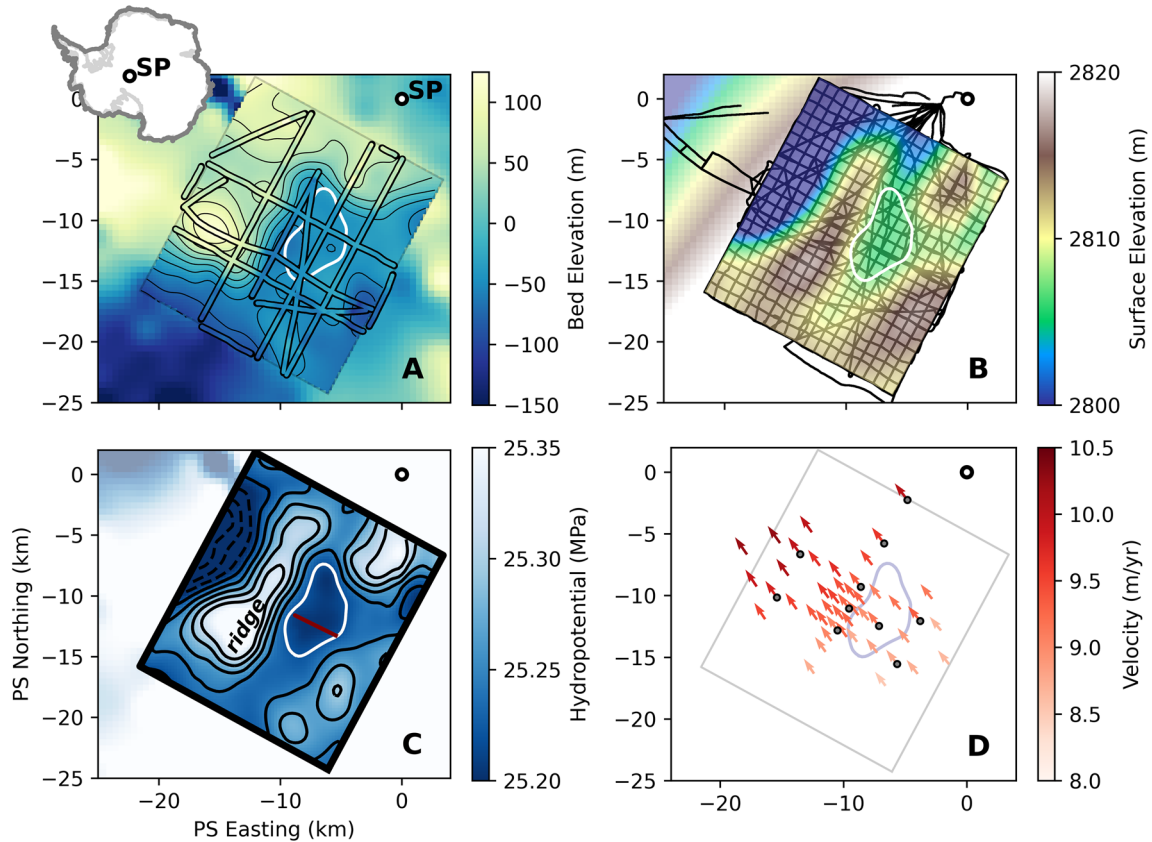
Figure 1. Maps of ice-sheet geometry at South Pole Lake (SPL) (projection EPSG:3031) (black dot is the geographic South Pole). (a) Bed geometry from deep-sounding radar. Colored lines are bed picks from the radar data presented in this study and the colored survey area is the interpolated bed elevation product. (b) Surface geometry from kinematic Global Navigation Satellite System (GNSS) data. The surveyed lines are in black, and the colored surface shows the interpolated surface elevation product. (c) Hydropotential calculated from (a) and (b). Black contours correspond to the colormap in the surveyed area with dashed below the interpreted lake level (white) and solid above. The maroon line shows the active-seismic survey location. In panels (a), (b), and (c), fields plotted outside the surveyed area are from reference products, the BedMachine bed elevation model (Morlighem et al., 2020) and REMA surface elevation model (Howat et al., 2019). (d) Surface velocity vectors measured with GNSS (red arrows) and sites of the 10 Autonomous phase-sensitive Radio Echo Sounder (ApRES) acquisitions (gray dots).

power inside and outside the lake area is 1.0 dB. The standard deviation of power for returns outside the lake area is 3.6 dB, and for those inside is 1.8 dB. The bed-echo power within the lake is statistically indistinguishable from its surrounding area.

2.3. Ice Dynamics

2.3.1. Surface Velocity and Strain Rates

Satellite surface velocity measurements are limited near the South Pole. Thus, we collected surface velocity measurements at 46 sites over the surveyed area by differencing repeat GNSS acquisitions over a time interval of 1 year (Figure 1d). Measurement locations (monuments) were marked using an aluminum pole driven ~20–30 cm into the snow surface. At each location, the GNSS antenna was attached to the monument using a removable mount and data were collected for a minimum of 10 min. The monument position for each measurement is the mean of all position solutions calculated from the 10-min measurement interval. Uncertainties are calculated as the standard deviation of the position solutions, which is ~2 cm in the horizontal dimensions. The mean velocity over the survey is 9.3 m/yr, with a slight increase from 8.5 to 10.3 m/yr in the direction of flow.

Using Delauney Triangulation, we grid the individual velocity measurements and calculate horizontal strain rates within each grid triangle (Jaeger, 1969; Shean et al., 2017). Tensile strain rates are as high as 2.5×10^{-4} yr^{-1}; compressive strain rates are slightly lower, up to 1.9×10^{-4} yr^{-1}. Measured surface strain is predominantly tensile
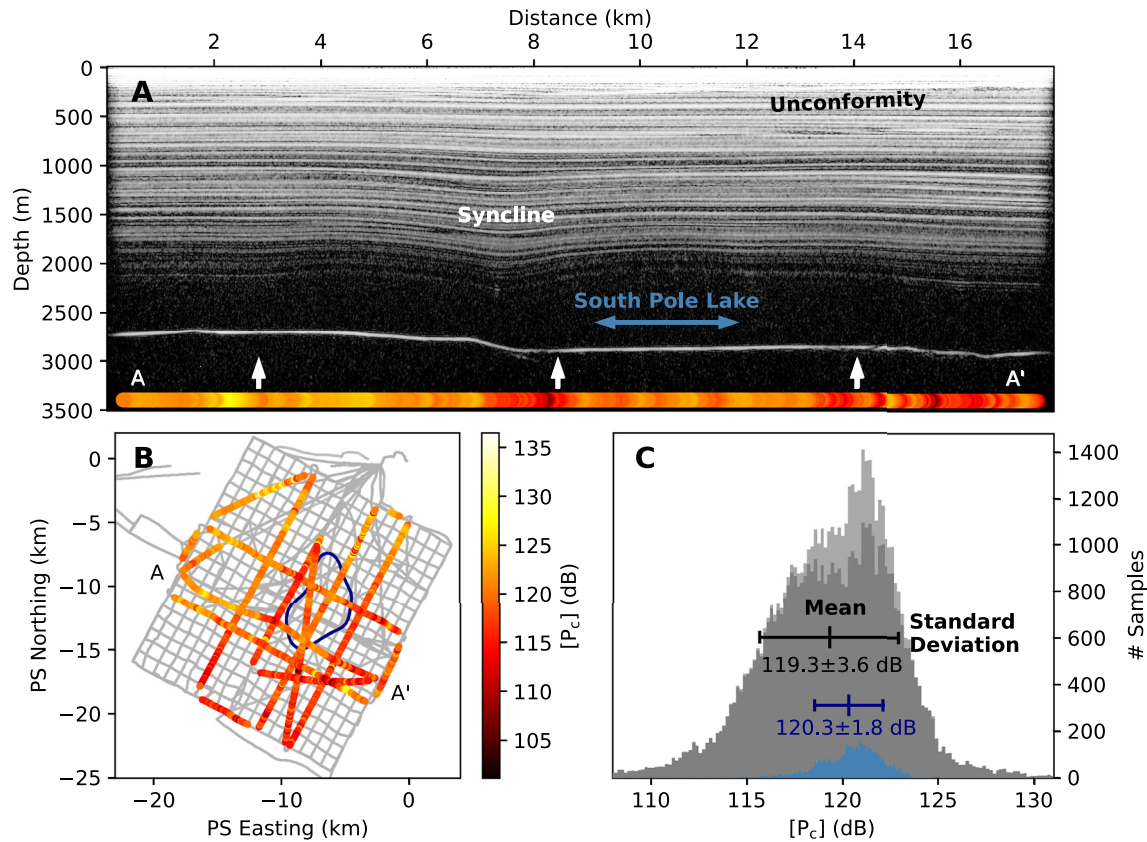
Figure 2. Deep-sounding radar power interpretation. (a) Radar profile with location in the survey shown by A-A′ in (b). Colored bar at the bottom shows the corrected bed-echo power for this profile, with amplitudes corresponding to the colorbar shown in (b). White arrows show the location of Autonomous phase-sensitive Radio Echo Sounder (ApRES) acquisitions. (b) Corrected bed-echo power for all radar lines overlain on the kinematic Global Navigation Satellite System (GNSS) survey (gray) and the interpreted lake outline (blue). (c) Bed-echo power for all traces over the radar survey (light gray), and for traces within (blue) and outside (dark gray) the interpreted lake area; mean (center hash mark) and standard deviation (edge hash marks) are shown for each.

along flow and compressive across flow. The highest tensile strain rates occur as ice flows over the ridge, and we do not distinguish any strong pattern in the strain rates associated with the lake boundary itself.

2.3.2. Englacial Vertical Velocity and Strain Rates

We calculate 10 vertical velocity profiles using repeat measurements from an Autonomous phase-sensitive Radio Echo Sounder (ApRES; Nicholls et al., 2015) collected over a 1-year interval. ApRES data are processed as described by Brennan et al. (2014) and implemented in ImpDAR (Lilien et al., 2020). For each acquisition, we stack at least 1,000 raw chirps and do a range conversion using the known transmit signal. Following Kingslake et al. (2014), we calculate phase uncertainty using a median noise phasor associated with the noise floor for returns from below the bed reflector. The observed layer deflection is the phase difference between acquisitions after converting to distance using the center frequency of the transmitted signal (300 MHz).

Due to characteristic changes between profiles, vertical velocity results are grouped by those measurements taken away from the ridge and those taken on top of it (Figure 3). Profiles away from the ridge have an approximately linear velocity profile extending from no movement at the bed to the known accumulation rate (~8.7 cm/yr) at the surface, which is expected for slow-flowing ice. The signal vanishes for reflections below ~2,000-m depth due to low phase coherence (<0.9) between acquisitions. Phase coherence is high (>0.9) at the bed reflection itself. Along the ridge, we observe ~2–3 times the vertical strain, with some variability between sites, and an apparent upward motion for deep reflections and the bed assuming the same accumulation rate as for sites off the ridge.
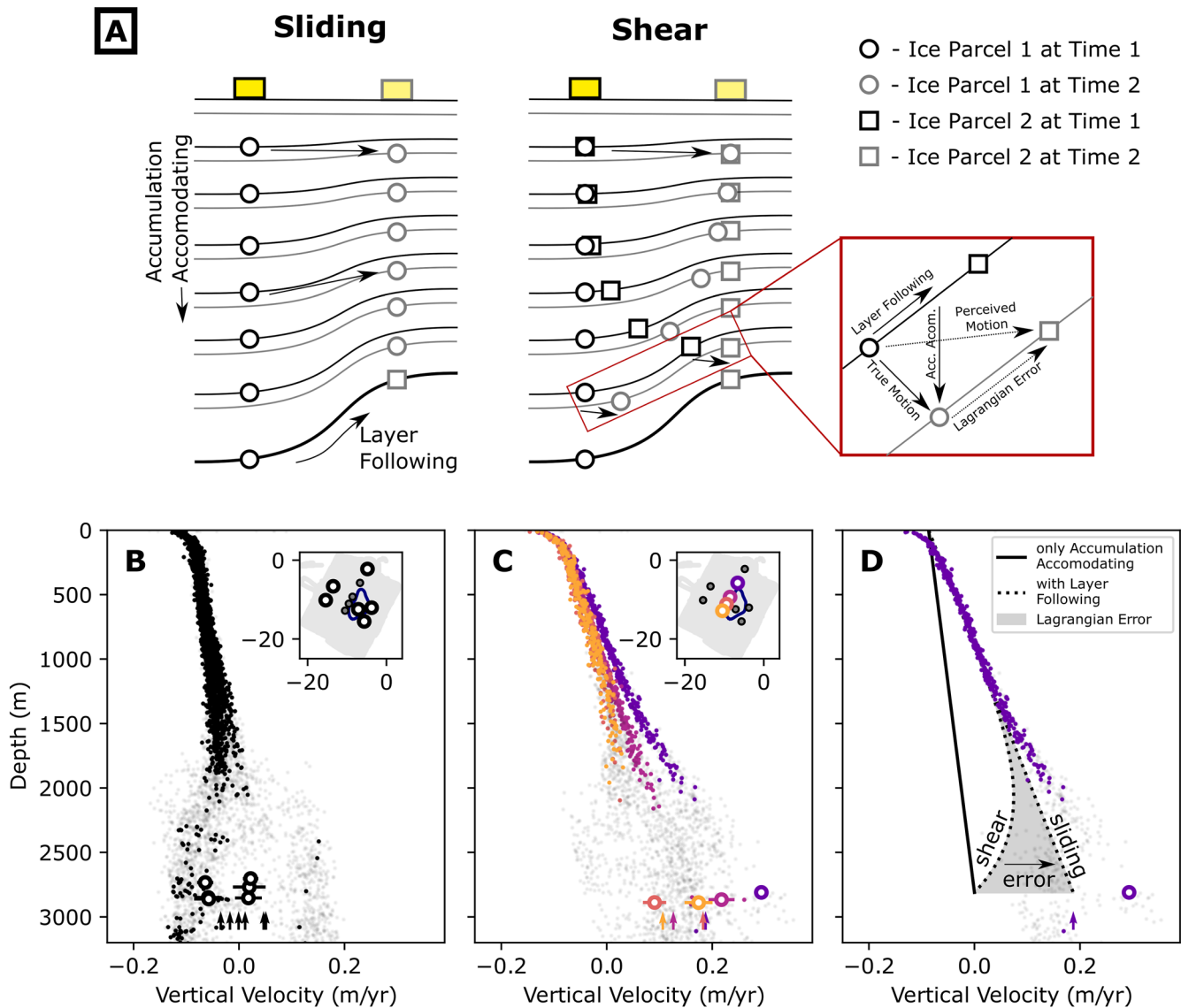
Figure 3. Vertical velocity interpretation. (a) An illustration of ice moving over a bedrock bump with reflection surfaces (black at the first acquisition and gray at the second), imaged particles (circles), and the Autonomous phase-sensitive Radio Echo Sounder (ApRES) instrument (yellow box). In the shear case, the imaged particle only travels part of the distance that the instrument does, so a secondary particle is shown as a square. (b) Vertical velocity profiles from six ApRES sites away from the ridge. Solid black dots show measured velocities for reflections with high coherence between acquisitions and faded black dots show those with lower coherence. Open circles show vertical velocity at the bed reflector with a horizontal line for uncertainty. Arrows show the inferred bed motion from the surface velocity against measured bed and surface slopes. The inset is an overview map with the lake outline and open circles at the six site locations. (c) Same as (b) but for the four ApRES sites along the ridge. (d) Vertical velocity at one site from (c), now with reference lines for the accumulation-accommodating and layer-following components of motion (Holschuh et al., 2017). Lagrangian error is only applicable in the shear case.

3. Ice Temperature Methods and Results

Next, we examine ice temperature using a 1.5-dimensional advection-diffusion model in which we parameterize longitudinal advection to account for colder temperatures originating upstream (Supporting Information S4). We assume a constant surface velocity (9.3 m/yr), geothermal flux (60 mW/m^2), and ice geometry, ignoring any possible Holocene thickening (Lilien et al., 2018; Figure S23 in Supporting Information S1). We vary the surface temperature and accumulation rate over time. The chosen geothermal flux minimizes model-data misfit and is within the uncertainty for what has been estimated in this region (Martos et al., 2017; Shen et al., 2020; Stål et al., 2021).
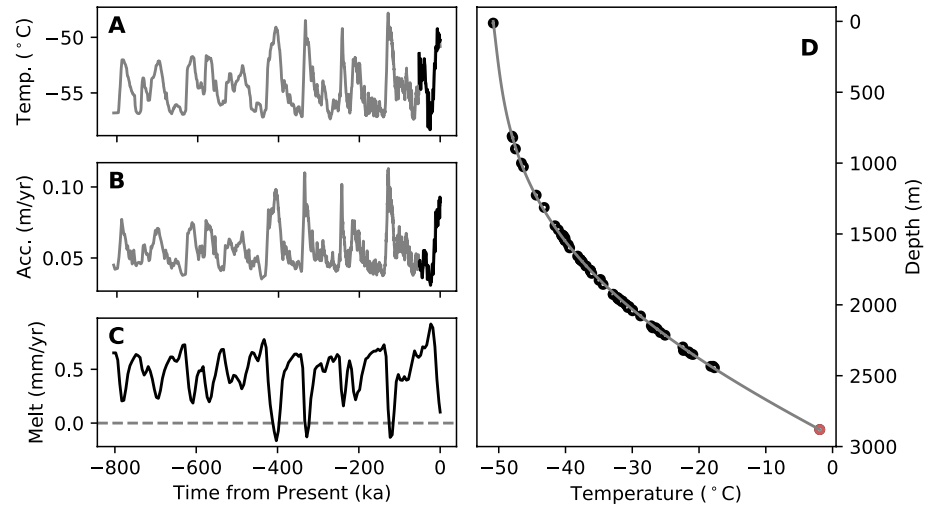
Figure 4. Temperature modeling data and results. (a) Surface temperature reconstruction from South Pole Ice Core (black) (Kahle et al., 2021) and scaled from EPICA Dome C (gray) (Jouzel et al., 2007). (b) Surface accumulation rate reconstructed from ice cores as in (a). (c) Modeled melt rates at South Pole Lake (SPL) with ice thickness of 2,852 m (black) and a reference line at 0 mm/yr basal melt (gray dashed). (d) Measured (black dots) and modeled (gray) ice temperature profiles. The shallowest data point is from nearby firn measurements (Giovineto, 1960) and the deepest point (displayed in red) is inferred at the pressure-melting point, assuming that the bed is thawed.

To constrain the surface boundary condition, we use reconstructions of temperature and accumulation rate from the South Pole Ice Core (Kahle et al., 2021). Ice-core data extend to only 50 ka before present, and our testing showed that the initial condition is still somewhat persistent over that time scale. Therefore, we extend the paleo-climate record using air temperature and accumulation data from EPICA Dome C (Jouzel et al., 2007). We scale these parameters to match the data from South Pole Ice Core using a regression over that 50-ka period (Figures 4a and 4b). We initialize the model to a steady-state temperature profile using a constant initial air temperature and accumulation rate (the initial value from each time series).

We first test the model against ice temperature measurements from the AMANDA/IceCube array (Price et al., 2002). Recent 7-MHz impulse radar data yields an ice thickness of approximately 2,880 m within the IceCube array (Figure S1 in Supporting Information S1), about 70 m deeper than previous estimates (Price et al., 2002). The best model-data fit is for basal sliding, where the vertical velocity profile is linear (Lliboutry (1979) shape factor, $p = 1,000$) and the shear stress is zero everywhere except the bed where it is approximated as equal to the driving stress. The resulting temperature profile matches the measurements to within $\pm 0.5°C$ and the ice-bed interface is thawed (Figure 4). In the internal shear case ($p \approx 10$), the heat source at the bed is weaker and shear heating in ice slightly above the bed is stronger, weakening the basal temperature gradient below what is observed (Figure S21 in Supporting Information S1). Hence, our model favors a velocity profile dominated by sliding rather than shear. Cooling from longitudinal advection is necessary to reproduce the observed temperatures; this is expected since the upstream temperatures are colder than those at South Pole (Fudge et al., 2020).

Next, we extend the modeling to the lake site. We assume that horizontal temperature gradients between the site of measured temperatures at the IceCube array and the lake are negligible, since strain rates are low and there is no liquid water present at the ice surface (cf. Hills et al., 2017). The ice thickness estimates are $2,852 \pm 10$ m above the lake. Again, we assume that the ice thickness and velocity are constant in time and that velocity is dominated by sliding. The resulting melt rate is positive through most of the reconstructed paleoclimate history with three brief exceptions during interglacial periods at 400, 320, and 120 ka. For some thinner areas around the lake, such as directly over the ridge, model results are colder and sometimes freezing at the bed. A small increase in the estimated geothermal flux (e.g., to 62 mW/m²) thaws the bed here, and nearby studies show that there is large uncertainty, with a geothermal flux as high as 120 mW/m² in one case (Jordan et al., 2018).

4. Discussion

Below, we argue that the geophysical data and ice temperature modeling suggest a regionally thawed bed for the region around the South Pole. Although inconclusive individually, taken together our arguments are only consistent with an interpretation of a thawed bed. Our result contradicts prior studies, which suggested that the bed is frozen (Beem et al., 2017; Price et al., 2002). Where appropriate, we point out these differences and indicate specifically what additional data led to our contrasting hypothesis.

The SPL lakestand is currently within 2 m of its capacity. If regional freeze-on had been persistent for the last 10,000 years at rates of at least 3 mm/yr, as suggested by Beem et al. (2017), we would expect the current lake level to be 30 m below its maximum capacity. A lake of a few meters depth would be at the limits of detectability (∼2 m water depth) using active-seismic methods (Horgan et al., 2012), whereas this lake is clearly detectable with 32 ± 10-m depth in active-seismic data (Peters et al., 2008).

Bed reflections are bright throughout the survey. The difference in mean bed power between reflections from inside and outside the lake area (1.0 dB) is well within the standard deviation over the entire survey (3.5 dB). If the area outside of the lake were frozen, we would expect the reflected power to decrease by ∼20 dB, which is the reflectivity difference between freshwater and frozen till/bedrock (Christianson et al., 2016; Peters et al., 2005). The bed power within the lake area has a slightly lower standard deviation than outside the lake, implying a more specular bed interface, which is expected for reflections from a likely smooth lake lid. A regionally bright bed is also consistent with radar data from the ITASE-2 traverse (Jacobel et al., 2010). Those data showed high bed-echo power in only two areas: Byrd Glacier and the last ∼250 km approaching the South Pole. If the fast-flowing Byrd Glacier has a thawed bed, the implication is that the bed near the South Pole is also thawed, corroborating our interpretation.

The upward motion measured in the vertical velocity profiles corresponds to ice flow over an upsloping bed at the ridge (Figure 3). To discuss these measurements, it is useful to separate the signal into three components: the accumulation-accommodating and the layer-following components of steady-state ice flow (Holschuh et al., 2017), and a Lagrangian error from horizontal motion of the ApRES instrument over a dipping reflector (i.e., the second acquisition images a different ice parcel along the same reflector). This error is only relevant in the shear case where velocities at depth are significantly slower than at the surface. Movement of the instrument itself over an upward dipping reflector leads to perceived upward motion. However, there is less bed parallel flow in this shear case, compensating for the error. Because of the Lagrangian error, we cannot directly distinguish between sliding and shear with any single vertical velocity profile, but together their uniformity and linearity suggest distributed sliding rather than discontinuous shear around the lake. There is also no substantial change in the surface strain rates across the lake boundary, which suggests that surface strain rates have minimal impact on spatial variability of vertical velocity.

Together, our temperature modeling and geophysical data interpretation suggest that for the present-day ice sheet: (a) sliding dominates over shear velocity; (b) the bed is currently thawed; and (c) the bed has been thawed for most of the past 800,000 years. The few times when modeled temperatures are close to or below freezing were during three brief interglacial periods with high accumulation. We have assumed that the higher accumulation was accommodated by additional vertical strain, but it is likely that the ice sheet thickened in response, which would decrease the amount of inferred freezing. All periods of modeled freezing were quickly followed by a rapid decline in the accumulation rate, which led to a return to basal melting.

The disagreement between previous studies (Beem et al., 2017; Price et al., 2002) and our temperature modeling is largely due to the updated ice thickness estimate of 2,880 m within the IceCube array. A thicker ice column usually has a warmer bed because it is better insulated from the cold surface. Even accounting for measurement uncertainty (∼¼ radar wavelength is 6 m at 7 MHz), this new, more direct ice-thickness measurement is still notably thicker than the previous estimates of 2,810 m (Price et al., 2002) and 2,800 m (Beem et al., 2017), which were based on the BedMap1 gridded product (Lythe & Vaughan, 2001). Since the best available ice thickness estimate is compatible with both the "cold" temperature measurements from IceCube and a thawed bed, our interpretation favors the simplest hypothesis; i.e., the ice-sheet bed is currently thawed and is thermodynamically stable in its present configuration.

Finally, we note that the seismic survey of SPL imaged 150 ± 60 m of sediment under the lake (Peters et al., 2008). The lake is therefore a viable drilling target for an East Antarctic sediment core, which could provide a paleoclimate record through many glacial cycles, as has been proposed for other subglacial lake sites (Smith et al., 2018). Sediments from a preserved Laurentide subglacial lake show that such a record could even persist between glaciations (Christoffersen et al., 2008). An ideal environment for an extended sediment record would be slow yet continuous deposition. While our data cannot guarantee the continuous presence of a thick water column, the modeled melt rates are positive through most of the 800-ka paleo reconstruction. Determining whether sediment deposition has been continuous, or if the lake has undergone periods of both deposition and erosion is beyond the scope of this work and would require more targeted geophysical surveys.

5. Conclusion

In this study, we present a geophysical survey at SPL. We find that the lake is currently full or nearly full of water to its maximum high stand given the current ice geometry, that the radar bed reflections are regionally bright, and that strain rates favor ice flow dominated by sliding as opposed to internal shear. Additionally, our temperature modeling, which is the most up-to-date model using high resolution estimates of ice thickness and the newly reconstructed paleoclimate variables from South Pole Ice Core, closely approximates the measured temperatures when assuming a sliding dominated velocity profile consistent with a thawed bed and some longitudinal advection. Based on these results, we argue that the ice-sheet bed is thawed in the area surrounding the South Pole and that SPL is therefore thermodynamically stable given the present-day ice-sheet geometry and climate. The deep sediment column, the apparent thermodynamic stability, and the basin's position on bedrock that would adjust to a surface well above sea-level in the absence of the East Antarctic Ice Sheet, establish the potential for the lake sediment to record a unique climate history potentially from the ice sheet's inception when SPL may have been open and exposed to the surface.

Data Availability Statement

The profiling radar data used in this article were first published in Hills et al. (2020); those, as well as the surface velocity measurements, ApRES acquisitions, and associated vertical velocities are all archived at https://www.usap-dc.org/view/project/p0010160. Radar processing software is available at https://github.com/dlilien/ImpDAR with a release version at https://doi.org/10.5281/zenodo.3251527. The temperature model is available at https://github.com/benhills/IceTemperature with a release version at https://doi.org/10.5281/zenodo.5831997.

References

Beem, L. H., Cavitte, M. G. P., Blankenship, D. D., Carter, S. P., Young, D. A., Muldoon, G. R., et al. (2017). Ice-flow reorganization within the East Antarctic ice sheet deep interior. *Geological Society, London, Special Publications*, *461*, 35–47. https://doi.org/10.1144/SP461.14

Bingham, R. G., Siegert, M. J., Young, D. A., & Blankenship, D. D. (2007). Organized flow from the South Pole to the Filchner-Ronne ice shelf: An assessment of balance velocities in interior East Antarctica using radio echo sounding data. *Journal of Geophysical Research*, *112*, F03S26. https://doi.org/10.1029/2006JF000556

Brennan, P. V., Lok, L. B., Nicholls, K., & Corr, H. (2014). Phase-sensitive FMCW radar system for high-precision Antarctic ice shelf profile monitoring. *IET Radar, Sonar & Navigation*, *8*, 776–786. https://doi.org/10.1049/iet-rsn.2013.0053

Carter, S. P., Blankenship, D. D., Peters, M. E., Young, D. A., Holt, J. W., & Morse, D. L. (2007). Radar-based subglacial lake classification in Antarctica. *Geochemistry, Geophysics, Geosystems*, *8*, Q03016. https://doi.org/10.1029/2006GC001408

Christianson, K., Jacobel, R. W., Horgan, H. J., Alley, R. B., Anandakrishnan, S., Holland, D. M., & Dallasanta, K. J. (2016). Basal conditions at the grounding zone of Whillans Ice Stream, West Antarctica, from ice-penetrating radar. *Journal of Geophysical Research: Earth Surface*, *121*, 1954–1983. https://doi.org/10.1002/2015JF003806

Christoffersen, P., Tulaczyk, S., Wattrus, N. J., Peterson, J., Quintana-Krupinski, N., Clark, C. D., & Sjunneskog, C. (2008). Large subglacial lake beneath the Laurentide Ice Sheet inferred from sedimentary sequences. *Geology*, *36*, 563–566. https://doi.org/10.1130/G24628A.1

Deconto, R. M., & Pollard, D. (2003). Rapid Cenozoic glaciation of Antarctica induced by declining atmospheric CO_2. *Nature*, *421*, 245–249. https://doi.org/10.1038/nature01290

Fudge, T. J., Lilien, D. A., Koutnik, M., Conway, H., Max Stevens, C., Waddington, E. D., et al. (2020). Advection and non-climate impacts on the South Pole ice core. *Climate of the Past*, *16*, 819–832. https://doi.org/10.5194/cp-16-819-2020

Giovineto, M. (1960). *South Pole shallow firn annual cycle temperatures, USNC-IGY Antarctic Glaciological Data, field work 1958 and 1959* (Report 825-2-Part IV, April 1960).

Hills, B. H., Christianson, K., & Holschuh, N. (2020). A framework for attenuation method selection evaluated with ice-penetrating radar data at South Pole Lake. *Annals of Glaciology*, *61*, 176–187. https://doi.org/10.1017/aog.2020.32

Hills, B. H., Harper, J. T., Humphrey, N. F., & Meierbachtol, T. W. (2017). Measured horizontal temperature gradients constrain heat transfer mechanisms in Greenland ice. *Geophysical Research Letters*, *44*, 9778–9785. https://doi.org/10.1002/2017GL074917

Holschuh, N., Parizek, B. R., Alley, R. B., & Anandakrishnan, S. (2017). Decoding ice sheet behavior using englacial layer slopes. *Geophysical Research Letters*, *44*, 5561–5570. https://doi.org/10.1002/2017GL073417

Horgan, H. J., Anandakrishnan, S., Jacobel, R. W., Christianson, K., Alley, R. B., Heeszel, D. S., et al. (2012). Subglacial Lake Whillans—Seismic observations of a shallow active reservoir beneath a West Antarctic ice stream. *Earth and Planetary Science Letters*, *331–332*, 201–209. https://doi.org/10.1016/j.epsl.2012.02.023

Howat, I. M., Porter, C., Smith, B. E., Noh, M.-J., & Morin, P. (2019). The reference elevation model of Antarctica. *The Cryosphere Discussions*, 1–16. https://doi.org/10.5194/tc-2018-240

Jacobel, R. W., Lapo, K. E., Stamp, J. R., Youngblood, B. W., Welch, B. C., & Bamber, J. L. (2010). A comparison of basal reflectivity and ice velocity in East Antarctica. *The Cryosphere*, *4*, 447–452. https://doi.org/10.5194/tc-4-447-2010

Jaeger, J. C. (1969). *Elasticity, fracture and flow*. Dordrecht, Netherland: Springer. https://doi.org/10.1007/978-94-011-6024-7

Jordan, T. A., Martin, C., Ferraccioli, F., Matsuoka, K., Corr, H., Forsberg, R., et al. (2018). Anomalously high geothermal flux near the South Pole. *Scientific Reports*, *8*, 16785. https://doi.org/10.1038/s41598-018-35182-0

Jouzel, J., Masson-Delmotte, V., Cattani, O., Dreyfus, G., Falourd, S., Hoffmann, G., et al. (2007). Orbital and millennial Antarctic climate variability over the past 800,000 years. *Science*, *317*, 793–796. https://doi.org/10.1126/science.1141038

Kahle, E. C., Steig, E. J., Jones, T. R., Fudge, T. J., Koutnik, M. R., Morris, V. A., et al. (2021). Reconstruction of temperature, accumulation rate, and layer thinning from an ice core at South Pole, using a statistical inverse method. *Journal of Geophysical Research: Atmospheres*, *126*, e2020JD033300. https://doi.org/10.1029/2020JD033300

Kingslake, J., Hindmarsh, R. C. A., Aðalgeirsdóttir, G., Conway, H., Corr, H. F. J., Gillet-Chaulet, F., et al. (2014). Full-depth englacial vertical ice sheet velocities measured using phase-sensitive radar. *Journal of Geophysical Research: Earth Surface*, *119*, 2604–2618. https://doi.org/10.1002/2014JF003275

Kuhn, G., Hillenbrand, C. D., Kasten, S., Smith, J. A., Nitsche, F. O., Frederichs, T., et al. (2017). Evidence for a palaeo-subglacial lake on the Antarctic continental shelf. *Nature Communications*, *8*, 15591. https://doi.org/10.1038/ncomms15591

Lilien, D. A., Fudge, T. J., Koutnik, M. R., & Conway, H. (2018). Holocene ice-flow speedup in the vicinity of the South Pole. *Geophysical Research Letters*, *45*, 6557–6565. https://doi.org/10.1029/2018GL078253

Lilien, D. A., Hills, B. H., Driscol, J., Jacobel, R., & Christianson, K. (2020). ImpDAR: An open-source impulse radar processor. *Annals of Glaciology*, *61*, 114–123. https://doi.org/10.1017/aog.2020.44

Lliboutry, L. (1979). A critical review of analytical approximate solutions for steady state velocities and temperatures in cold ice-sheets. *Zeitschrift für Gletscherkunde und Glazialgeologie*, *35*(2), 135–148.

Lythe, M. B., & Vaughan, D. G. (2001). Bedmap: A new ice thickness and subglacial topographic model of Antarctica. *Journal of Geophysical Research*, *106*, 11335–11351. https://doi.org/10.1029/2000JB900449

MacGregor, J. A., Winebrenner, D. P., Conway, H., Matsuoka, K., Mayewski, P. A., & Clow, G. D. (2007). Modeling englacial radar attenuation at Siple Dome, West Antarctica, using ice chemistry and temperature data. *Journal of Geophysical Research*, *112*, F03008. https://doi.org/10.1029/2006JF000717

Martos, Y. M., Catalán, M., Jordan, T. A., Golynsky, A., Golynsky, D., Eagles, G., & Vaughan, D. G. (2017). Heat flux distribution of Antarctica unveiled. *Geophysical Research Letters*, *44*, 11417–11426. https://doi.org/10.1002/2017GL075609

Morlighem, M., Rignot, E., Binder, T., Blankenship, D., Drews, R., Eagles, G., et al. (2020). Deep glacial troughs and stabilizing ridges unveiled beneath the margins of the Antarctic ice sheet. *Nature Geoscience*, *13*, 132–137. https://doi.org/10.1038/s41561-019-0510-8

Nicholls, K. W., Corr, H. F. J., Stewart, C. L., Lok, L. B., Brennan, P. V., & Vaughan, D. G. (2015). Instruments and methods: A ground-based radar for measuring vertical strain rates and time-varying basal melt rates in ice sheets and shelves. *Journal of Glaciology*, *61*, 1079–1087. https://doi.org/10.3189/2015JoG15J073

Peters, L. E., Anandakrishnan, S., Holland, C. W., Horgan, H. J., Blankenship, D. D., & Voigt, D. E. (2008). Seismic detection of a subglacial lake near the South Pole, Antarctica. *Geophysical Research Letters*, *35*, L23501. https://doi.org/10.1029/2008GL035704

Peters, M. E., Blankenship, D. D., & Morse, D. L. (2005). Analysis techniques for coherent airborne radar sounding: Application to West Antarctic ice streams. *Journal of Geophysical Research*, *110*, B06303. https://doi.org/10.1029/2004JB003222

Price, P. B., Nagornov, O. V., Bay, R., Chirkin, D., He, Y., Miocinovic, P., et al. (2002). Temperature profile for glacial ice at the South Pole: Implications for life in a nearby subglacial lake. *Proceedings of the National Academy of Sciences of the United States of America*, *99*, 7844–7847. https://doi.org/10.1073/pnas.082238999

Shean, D. E., Christianson, K., Larson, K. M., Ligtenberg, S. R. M., Joughin, I. R., Smith, B. E., et al. (2017). GPS-derived estimates of surface mass balance and ocean-induced basal melt for Pine Island Glacier ice shelf, Antarctica. *The Cryosphere*, *11*, 2655–2674. https://doi.org/10.5194/tc-11-2655-2017

Shen, W., Wiens, D. A., Lloyd, A. J., & Nyblade, A. A. (2020). A geothermal heat flux map of Antarctica empirically constrained by seismic structure. *Geophysical Research Letters*, *47*, e2020GL086955. https://doi.org/10.1029/2020GL086955

Shreve, R. L. (1972). Movement of water in glaciers. *Journal of Glaciology*, *11*, 205–214. https://doi.org/10.3189/S002214300002219X

Siegert, M. J. (2008). Antarctic subglacial topography and ice-sheet evolution. *Earth Surface Processes and Landforms*, *33*, 646–660. https://doi.org/10.1002/esp

Siegert, M. J., Carter, S., Tabacco, I., Popov, S., & Blankenship, D. D. (2005). A revised inventory of Antarctic subglacial lakes. *Antarctic Science*, *17*, 453–460. https://doi.org/10.1017/S0954102005002889

Smith, A. M., Woodward, J., Ross, N., Bentley, M. J., Hodgson, D. A., Siegert, M. J., & King, E. C. (2018). Evidence for the long-term sedimentary environment in an Antarctic subglacial lake. *Earth and Planetary Science Letters*, *504*, 139–151. https://doi.org/10.1016/j.epsl.2018.10.011

Stål, T., Reading, A. M., Halpin, J. A., & Whittaker, J. M. (2021). Antarctic geothermal heat flow model: Aq1. *Geochemistry, Geophysics, Geosystems*, *22*, e2020GC009428. https://doi.org/10.1029/2020GC009428

Steig, E. J., Jones, T. R., Schauer, A. J., Kahle, E. C., Morris, V. A., Vaughn, B. H., et al. (2021). Continuous-flow analysis of $\delta^{17}O$, $\delta^{18}O$, and δD of H_2O on an ice core from the South Pole. *Frontiers of Earth Science*, *9*, 640292. https://doi.org/10.3389/feart.2021.640292

Tikku, A. A., Bell, R. E., Studinger, M., & Clarke, G. K. C. (2004). Ice flow field over Lake Vostok, East Antarctica inferred by structure tracking. *Earth and Planetary Science Letters*, *227*, 249–261. https://doi.org/10.1016/j.epsl.2004.09.021

References From the Supporting Information

Corr, H., Ferraccioli, F., Jordan, T., & Robinson, C. (2021). *Processed airborne radio-echo sounding data from the AGAP survey covering Antarctica's Gamburtsev Province, East Antarctica (2007/2009)* (Version 1.0). NERC EDS UK Polar Data Centre. https://doi.org/10.5285/A1ABF071-85FC-4118-AD37-7F186B72C847

Corr, H. F. J., Ferraccioli, F., Frearson, N., Jordan, T., Robinson, C., Armadillo, E., et al. (2007). Airborne radio-echo sounding of the Wilkes subglacial basin, the Transantarctic Mountains and the Dome C region. *Terra Antartica Reports*, *13*, 55–63.

Cuffey, K., & Paterson, W. S. B. (2010). *The Physics of Glaciers* (4th ed.). Butterworth-Heinemann.

Glen, J. W. (1952). Experiments on the deformation of ice. *Journal of Glaciology*, *2*, 111–114. https://doi.org/10.3189/S0022143000034067

Looyenga, H. (1965). Dielectric constants of heterogeneous mixtures. *Physica*, *31*(3), 401–406. https://doi.org/10.1016/0031-8914(65)90045-5

Schwerdtfeger. (1963). Theoretical derivation of the thermal conductivity and diffusivity of snow. *International Association of Scientific Hydrology*, *61*, 75–81.

Uieda, L., Tian, D., Leong, W. J., Jones, M., Schlitzer, W., Toney, L., et al. (2021). PyGMT: A Python interface for the generic mapping tools. *Zenodo* (Computer Software). https://doi.org/10.5281/zenodo.5607255

Weertman, J. (1968). Comparison between measured and theoretical temperature profiles of the Camp Century, Greenland, Borehole. *Journal of Geophysical Research*, *73*(8), 2691–2700. https://doi.org/10.1029/JB073i008p02691

Welch, B. C., & Jacobel, R. W. (2003). Analysis of deep-penetrating radar surveys of West Antarctica, US-ITASE 2001. *Geophysical Research Letters*, *30*(8). https://doi.org/10.1029/2003GL017210

Winski, D. A., Fudge, T. J., Ferris, D. G., Osterberg, E. C., Fegyveresi, J. M., Cole-Dai, J., et al. (2019). The SP19 chronology for the South Pole Ice Core—Part 1: Volcanic matching and annual layer counting. *Climate of the Past*, *15*(5), 1793–1808. https://doi.org/10.5194/cp-15-1793-2019